Interacting resonance effects along an isoelectronic sequence: Electron-impact excitation of Mg-like ions

N. R. Badnell

Department of Physics and Applied Physics, University of Strathclyde, Glasgow G4 0NG, United Kingdom

D. C. Griffin

Department of Physics, Rollins College, Winter Park, Florida 32789

T. W. Gorczyca and M. S. Pindzola

Department of Physics, Auburn University, Auburn, Alabama 36849

We have carried out a series of isolated-resonance and R-matrix close-coupling calculations for the electron-impact excitation of the $3s^2\,^1S \rightarrow 3s3p\,^3P$ transition in the Mg-like ions Ar^{6+}, Ti^{10+}, Fe^{14+}, and Se^{22+}. We obtain good agreement between the results of the two theoretical methods for three-state calculations, i.e., for the description of just a single Rydberg series of resonances. However, when two or more Rydberg series are present we observe large differences, due to interacting resonance effects, over a wide range of energies for all of the ions examined. For the case of Fe^{14+}, we have continued the perturbative studies of interacting resonances of Griffin *et al.* [Phys. Rev. Lett. **72**, 3491 (1994)] and also find the predominant effect to be due to direct configuration interaction between the resonant states rather than being due to their coupling through a common continuum. Our inclusion of these interacting resonance effects removes the major discrepancies between the perturbative and nonperturbative results for Fe^{14+} reported previously [Badnell *et al.*, Phys. Rev. A **48**, R2519 (1993)]. This is of importance for the study of indirect processes which are strongly radiation damped, for which the perturbative approach is widely used and the standard formulation of the close-coupling approximation is not applicable.

PACS number(s): 34.80.Kw

I. INTRODUCTION

Resonant processes frequently dominate low-energy electron-ion collision cross sections and, via the tail of the Maxwellian distribution function, strongly affect the level populations of ions and hence plasma diagnostics over a wide range of temperatures and densities. The standard R-matrix approach [1] to atomic collisions has largely superseded the nonresonant distorted-wave method due to its efficient solution of the close-coupling equations and its inclusion of resonances; the latter is of more importance for multiply charged ions, particularly as the nonresonant cross section scales as Z^{-4} while the resonant contribution scales as Z^{-3} (at least initially). The lack of explicit coupling to the atomic radiation field in the standard R-matrix approach, however, means that resonance widths are determined purely by their autoionizing width (except near the Rydberg limit where the Gailitis average can be applied [2]). So for "sufficiently" highly charged ions the resonance contribution is grossly overestimated [3]. This is true both for the electron-electron and electron-photon scattering channels, in the latter case, this neglect of the radiative width is sometimes referred to as the weak-field approximation [4]. For example, radiation damping reduces the excitation-autoionization contribution to the ionization of Fe^{15+} by 40% and the dielectronic-capture double-autoionization contribution by a factor of 2. In Fe^{23+} this rises to about a factor of 3, in Kr^{33+} a factor of 6, and Xe^{51+} a factor of 25, while

Be-like and B-like ions, etc., show similar reductions. Also, dielectronic recombination cross sections are reduced by radiation damping (in the width) by a factor of 6 and 20 for the $2\,^3S$ and $2\,^1S$ metastable states of N^{5+}, a factor of 5 for $\delta n = 0$ transitions in Ar^{15+}, and a factor of 300 for $\delta n = 1$ transitions in Se^{25+}, for example. Consequently, an alternative (perturbative) approach has been pursued for highly charged (and not so highly charged) ions, namely the independent-processes and isolated-resonance approximation using distorted waves (denoted the IPIRDW approximation). It is straightforward to allow for all types of radiation damping transitions within the IPIRDW approximation [5]. It has long been known that distorted waves are generally a good approximation for an electron scattering off of an ion that is several times ionized [6]. More recently, we have shown that interference effects between the resonant and nonresonant contributions to electron-impact excitation diminish rapidly as the charge state increases [7]; only dipole transitions in near neutral ions retain a strong enough background to interfere strongly with the resonant contribution, which is small in this case. In the case of electron-ion recombination we have shown that the interference between dielectronic and radiative recombination is almost always negligible [8]. Thus we have now begun to explore the validity of the isolated-resonance approximation [8,9]. Recently, we carried out a series of isolated-resonance and R-matrix close-coupling (CCR) calculations for the electron-impact excitation of the $3s^2\,^1S \rightarrow 3s3p\,^3P$ transition in Fe^{14+}, using the same

atomic structure, and demonstrated the apparent breakdown of the isolated-resonance approximation [9]. Furthermore, we have begun to investigate the nature of interacting resonances using perturbative interacting resonance theory [10]. In this paper, we present the results of an isoelectronic study of the apparent breakdown of the isolated-resonance approximation for the electron-impact excitation of Mg-like ions and analyze selected resonance structures in the $3s^2\,{}^1S \rightarrow 3s3p\,{}^3P$ cross section of Fe^{14+}. This sequence is one which we had begun to study in connection with electron energy-loss spectroscopy experiments at Oak Ridge National Laboratory, and consisted only of R-matrix results for Si^{2+} and Ar^{6+} [11].

The layout of the paper is as follows. In Sec. II we describe the theory behind the isolated-resonance, perturbative interacting resonance, and CCR calculations. In Sec. III we present and discuss our results while in Sec. IV we draw our conclusions.

II. THEORY

In the independent-processes approximation [5], the total excitation cross section σ_T from an initial state i to a final state f is given by

$$\sigma_T(i \rightarrow f) = \sigma_{NR}(i \rightarrow f) + \sigma_{RE}(i \rightarrow f) , \tag{1}$$

where $\sigma_{NR}(i \rightarrow f)$ is the nonresonant background cross section and $\sigma_{RE}(i \rightarrow f)$ is the resonant-excitation cross section. We note that it is possible to allow perturbatively for interference between the resonant and nonresonant processes. However, in its simplest representation this interference term vanishes identically when energy averaged [12] and we do not consider it further. In the isolated-resonance approximation, the resonant-excitation cross section at an incident energy k_i^2 is given by

$$\sigma_{RE}(i \rightarrow f) = \frac{(a_0\hbar)^2\pi}{k_i^2} \sum_j \frac{\omega_j}{2\omega_i} \frac{A_a(j \rightarrow i)A_a(j \rightarrow f)}{(E - E_j)^2 + \frac{1}{4}\Gamma_j^2} , \tag{2}$$

where the total width Γ_j is given by

$$\Gamma_j = \hbar \sum_{g,h} A_a(j \rightarrow h) + A_r(j \rightarrow g) . \tag{3}$$

Here, the autoionization rate A_a is given by

$$A_a(j \rightarrow i) = \frac{8I_H}{\hbar} |\langle i|V|j \rangle|^2 , \tag{4}$$

with the electrostatic operator V given by

$$V = \sum_{s=1}^{N} \frac{1}{|\mathbf{r}_s - \mathbf{r}_{N+1}|} , \tag{5}$$

and the radiative rate A_r is given by

$$A_r(j \rightarrow g) = 2\pi |\langle g|D|j \rangle|^2 , \tag{6}$$

where D is the electric dipole interaction given by

$$D = \left[\frac{2}{3\pi\tau_0\omega_j} \left[\frac{\alpha(E_j - E_k)}{2I_H} \right]^3 \right]^{1/2} P , \tag{7}$$

where P is the dipole moment with polarization $\hat{\epsilon}$,

$$P = \sum_{s=1}^{N+1} \mathbf{r}_s \cdot \hat{\epsilon}_s . \tag{8}$$

Finally, ω_j is the statistical weight of the $(N+1)$-electron doubly excited state j with energy E_j, ω_i is the statistical weight of the N-electron initial state i with energy E_i, and I_H is the ionization potential of the hydrogen atom. The continuum normalization is taken to be $k^{-1/2}$ times a sine function [13]. In general, the states $\langle i|$ are configuration mixed, i.e., $\langle i| = \langle i|t \rangle\langle t|$ where $\langle t|$ denotes our initial basis. In LS coupling $t = C\beta SL\pi$ while in intermediate coupling $t = C\beta SLJ\pi$ (see Refs. [14,15] for further details).

We identify two aspects of the interacting resonance problem, viz., direct configuration mixing, which is of order V in perturbation theory, and interactions through common continua, which are of order V^2. Direct configuration mixing is included within the close-coupling formalism through interactions between closed channels. However, in the IPIRDW approximation, direct configuration mixing is included within the N-electron target states but is generally neglected between the $(N+1)$-electron autoionizing states, excepting parental mixing or the case of low-lying resonances, e.g., KLL, MNN, etc. The reason for this is that in principle it would be necessary to diagonalize a Hamiltonian containing an entire Rydberg series of states; in practice, a preliminary pass through the resonant states would identify $SL\pi$ or $J\pi$ states that were close enough in energy to warrant subsequent interaction. This is in effect the approach that we take in this paper to evaluate direct configuration mixing, albeit with pairs of resonances at a time for one transition in one ion for now.

In addition, resonance interactions through common continua can be evaluated perturbatively using Feshbach theory [16]. In this case, the resonant-excitation cross section is given by

$$\sigma_{RE}(i \rightarrow f) = \frac{32\pi a_0^2 I_H^2}{\omega_i k_i^2} \left| \sum_{j,k} \frac{\omega_j^{1/2}\langle f|V|k \rangle(\Omega^{-1})_{kj}\langle j|V|i \rangle}{(E - E_j) + \frac{i}{2}\Gamma_j} \right|^2 , \tag{9}$$

where the elements of the dimensionless coupling matrix Ω are given by

$$\Omega_{kj} = \delta_{kj} - (1 - \delta_{kj}) \frac{\Lambda_{kj}}{E - E_k + \frac{i}{2}\Gamma_k} . \tag{10}$$

In the pole approximation,

$$\Lambda_{kj} = -\frac{i\hbar}{2} [\tilde{A}_a(k \rightarrow j) + \tilde{A}_r(k \rightarrow j)] , \tag{11}$$

where the generalized autoionization coupling rate is

given by

$$\tilde{A}_a(k \rightarrow j) = \frac{8I_H}{\hbar} \sum_i \langle j|V|i \rangle \langle i|V|k \rangle \ , \qquad (12)$$

and the generalized radiative coupling rate is given by

$$\tilde{A}_r(k \rightarrow j) = 2\pi \sum_g \langle j|D|g \rangle \langle g|D|k \rangle \ . \qquad (13)$$

We note that Eq. (9) corresponds to the one that we used in our study of interacting resonances in dielectronic recombination [8], except there $\langle f|V|k \rangle$ was replaced by $\langle g|D|k \rangle$ where g denotes a photon continuum rather than an electron continuum f. We note that the isolated-resonance approximation is recovered on setting $\Omega_{jk} = \delta_{jk}$ in Eq. (9), since $\Lambda_{jk} = \delta_{jk}\Lambda_{jk}$ in Eq. (10) for noninteracting resonances.

The solution of the close-coupling equations for electron-impact excitation at closed-channel energies automatically generates interacting Feshbach resonances. We make use of the R-matrix method to solve the close-coupling equations [1]. Here, the total $(N + 1)$-electron wave function is expanded, in an inner region that encloses the ion, in terms of a finite set of bound-continuum and bound-bound functions; the latter are included both to satisfy the orthogonality conditions imposed on the former and, optionally, to allow for electron-electron correlation. For the ions considered here, we found that including configurations beyond those required by orthogonality had a negligible effect on the collision results. The continuum function is expanded additionally in terms of a finite set of basis functions that are independent of the scattering energy; it is this feature that facilitates the solution of the scattering problem at the many thousands of energies that are required to delineate the resonance structure. The continuum expansion coefficients are determined by a diagonalization of the $(N + 1)$-electron Hamiltonian within the inner region and by the imposition of suitable boundary conditions. We make use of the nonrelativistic R-matrix program developed for the Opacity Project [17]. This version of the R-matrix program treats the long-range coupling terms in the outer region perturbatively. However, below each new excitation threshold the existing numerical approach breaks down and so the perturbative corrections are turned off automatically until the new threshold opens up. Although this is of little importance for total rate coefficients, it results in a step function in the cross section at each new threshold. In the Appendix to this paper, we show how to reformulate the solution in the outer region so that the perturbative corrections can be applied at all energies.

The perturbative (IPIRDW and IPDW) calculations of the resonant-excitation cross section were carried out using the AUTOSTRUCTURE computer program [15,18] which Schmidt-orthogonalizes the continuum and Rydberg orbitals to the target and/or core orbitals and neglects the effects of the $3l3l'3l''$ configurations on the remaining collision problem. We found that the IPIRDW threshold partial collision strengths for the $3s^2\,^1S \rightarrow 3s3d\,^{1,3}D$ and $3s3p\,^3P \rightarrow 3s3d\,^{1,3}D$ transitions differed by less than 20% from those of the CCR calcula-

tion, the largest differences arising on the smallest partial-wave contributions. All of the calculations were carried out in the LS-coupling scheme. The nonresonant contribution to the excitation cross section was calculated by combining the free-free collision algebra of STG2 of the R-matrix codes [17] with nonorthogonal atomic and continuum distorted-wave radial functions.

We used the same nonrelativistic N-electron atomic structure in both our perturbative and CCR calculations. We generated the 13-term configuration interaction target expansion arising from the $3s^2$, $3s3p$, $3s3d$, $3p3d$, and $3d^2$ configurations using the multiconfiguration Hartree-Fock programs of Froese Fischer [19], the orbitals for which were generated from a single configuration Hartree-Fock approximation. We then adjusted the resulting term energies to the $(2J + 1)$ weighted average of the observed energies [20], for both sets of collision calculations. In the CCR calculations these corrections are added to the diagonal of the $(N + 1)$-electron Hamiltonian before its diagonalization. In the case of the IPIRDW calculations it makes little difference whether the corrections are made before or after diagonalization of the said Hamiltonian since virtually all of the configuration mixing takes place within the N-electron core. In the perturbative direct configuration mixing calculations it is important to adjust the target (and thus core) energies before diagonalization of the $(N + 1)$-electron Hamiltonian.

III. RESULTS

We now present the results of a series of IPIRDW and CCR calculations for the electron-impact excitation of the $3s^2\,^1S \rightarrow 3s3p\,^3P$ transition in Ar^{6+}, Ti^{10+}, Fe^{14+}, and Se^{22+}. Care was taken to ensure that the CCR resonances were sufficiently energy resolved so as to give a converged result when convoluted with a 0.25–1.0 eV full width at half maximum (FWHM) Gaussian function (depending on the ion in question). The IPIRDW resonances were energy-averaged analytically before convolution and so there is no resolution problem in this approximation. In Fig. 1 we present our three-state results for the leading resonances of the $3s3d\,^3Dnl$ Rydberg series present in the $3s^2\,^1S \rightarrow 3s3p\,^3P$ excitation cross section for Ar^{6+}. We see that the IPIRDW and CCR results are in good agreement. Similarly, we present three-state IPIRDW and CCR results for the leading resonances of the $3s3d\,^1Dnl$ and $3s3p\,^1Pnl$ Rydberg series in Figs. 2 and 3, and five-state results showing the leading resonances of the $3p^2$ (^1S, ^3P and ^1D)nl series in Fig. 4. Again, we find good agreement between the IPIRDW and CCR results. Figure 4 indicates that there is little interaction between the three Rydberg series attached to the terms of the $3p^2$ configuration. As expected from our earlier work [7], interference effects between the resonant and nonresonant contributions are small. However, in Fig. 5 we show the net result of all of the interacting resonances in a comparison of eight-state ($3s^2\,^1S$, $3s3p\,^{1,3}P$, $3s3d\,^{1,3}D$, and $3p^2\,^1S, ^3P, ^1D$) IPIRDW and CCR results. The IPIRDW results are merely a superposition of the results shown in Figs. 1–4 while the CCR results allow for interaction between the various series of resonances. We observe
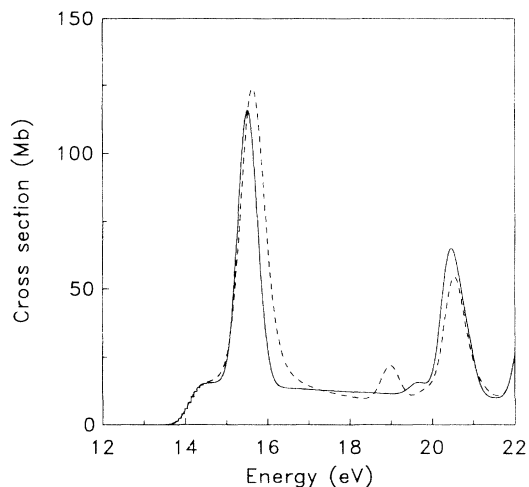
FIG. 1. Electron-impact excitation cross sections for the $3s^2\,^1S \to 3s3p\,^3P$ transition in Ar^{6+}, convoluted with a 0.25-eV FWHM Gaussian function. Three-state calculations including the $3s3d\,^3D$ term; ——, IPIRDW results; ----, CCR results; both this work.
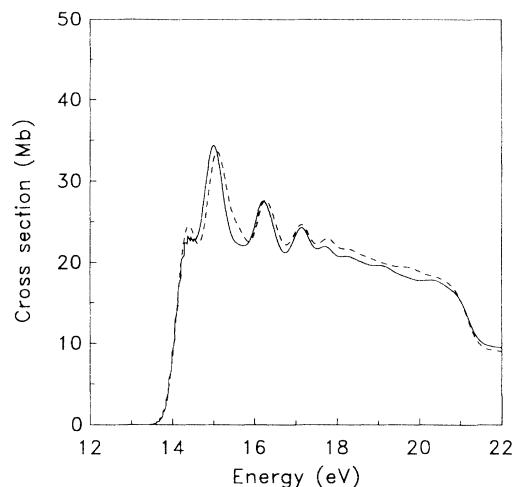

FIG. 3. Electron-impact excitation cross sections for the $3s^2\,^1S \to 3s3p\,^3P$ transition in Ar^{6+}, convoluted with a 0.25-eV FWHM Gaussian function. Three-state calculations including the $3s3p\,^1P$ term; ——, IPIRDW results; ----, CCR results; both this work.

widespread differences over the entire energy range shown; factors of 2 and 3 differences between the strongest resonance features are noted. There is little of interest to see above 21 eV because the $3s3p\,^1P$ channel opens up then and suppresses resonances in the $3s3p\,^3P$ channel.

We have carried out similar studies of three- and five-state calculations for the other ions, and the results of a detailed analysis have already been presented for Fe^{14+} [9]. However, it is of interest here only to present the final eight-state results to illustrate the widespread effects of interacting resonances. Thus we present our eight-

state results for Ti^{10+}, Fe^{14+}, and Se^{22+} in Figs. 6–8, respectively; the Fe^{14+} results are included as they are to be the subject of a detailed study below. Typically, we see factors of 2 or 3 difference between resonance peak heights. There is no obvious isoelectronic trend, although we note that the Se^{22+} results (Fig. 8) show the smallest differences between the IPIRDW and CCR results. As expected, radiation damping effects are small for this $\delta n = 0$ outer shell excitation (about 5% for Se^{22+}).

We now look in more detail at the nature of interacting

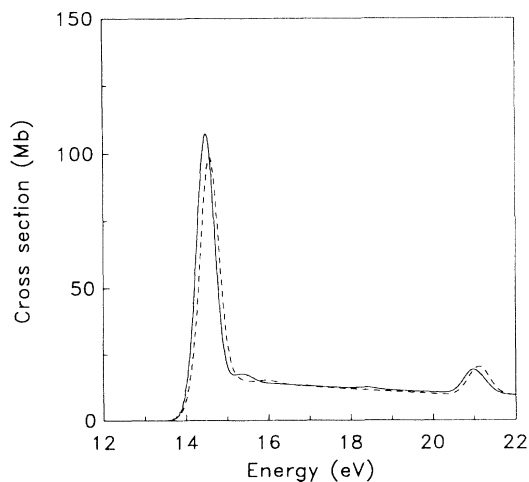FIG. 2. Electron-impact excitation cross sections for the $3s^2\,^1S \to 3s3p\,^3P$ transition in Ar^{6+}, convoluted with a 0.25-eV FWHM Gaussian function. Three-state calculations including the $3s3d\,^1D$ term; ——, IPIRDW results; ----, CCR results; both this work.
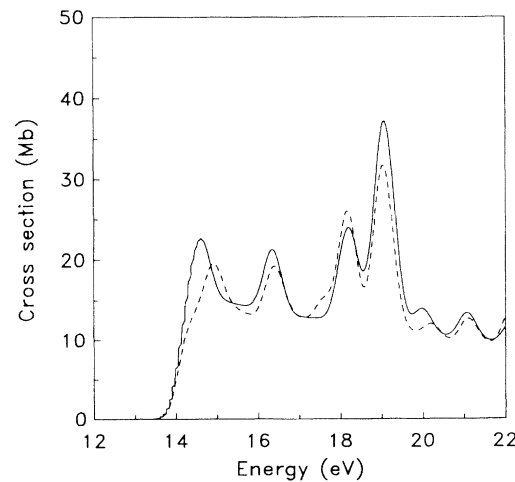

FIG. 4. Electron-impact excitation cross sections for the $3s^2\,^1S \to 3s3p\,^3P$ transition in Ar^{6+}, convoluted with a 0.25-eV FWHM Gaussian function. Five-state calculations including the $3p^2\,^1S$, ^3P, and ^1D terms; ——, IPIRDW results; ----, CCR results; both this work.
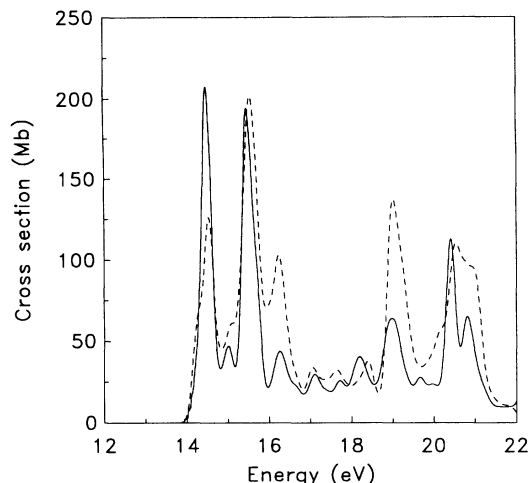
FIG. 5. Electron-impact excitation cross sections for the $3s^2\,^1S\rightarrow 3s3p\,^3P$ transition in Ar^{6+}, convoluted with a 0.25-eV FWHM Gaussian function. Eight-state calculations including the $3s^2\,^1S$, $3s3p\,^{1,3}P$, $3s3d\,^{1,3}D$, and $3p^2\,^1S$, ^3P, and ^1D terms; ——, IPIRDW results; ----, CCR results; both this work.

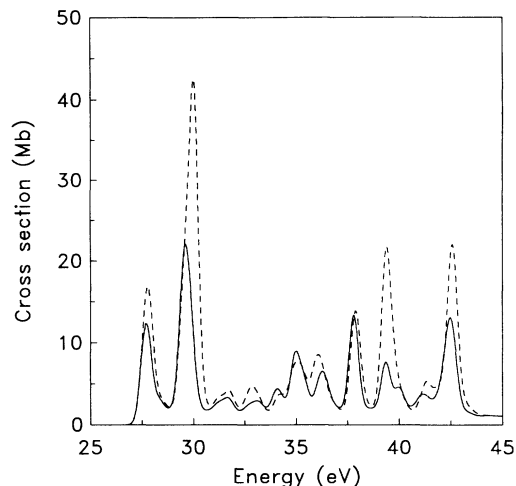FIG. 7. Electron-impact excitation cross sections for the $3s^2\,^1S\rightarrow 3s3p\,^3P$ transition in Fe^{14+}, convoluted with a 0.5-eV FWHM Gaussian function. Eight-state calculations including the $3s^2\,^1S$, $3s3p\,^{1,3}P$, $3s3d\,^{1,3}D$, and $3p^2\,^1S$, ^3P, and ^1D terms; ——, IPIRDW results; ----, CCR results; both this work.

resonance effects, and for the case of Fe^{14+} in particular. We see from Fig. 7 that the largest interacting resonance effects occur for the structures at about 29 eV, 39 eV and, to a lesser extent, 42.5 eV. The structure at 39 eV is due to the resonances $3s3d(^1D)7f\,^2F^o$ and $3s3d(^3D)8p\,^2F^o$, i.e., the differences are confined to a single symmetry. In Fig. 9 we present our four-state IPIRDW and CCR results for this $^2F^o$ symmetry without any convolution of the cross section; the resonance lying at the higher energy is the $3s3d(^1D)7f\,^2F^o$. In Fig. 10 we present our perturbative interacting resonance results that allow for direct

configuration mixing between the two resonances concerned, but neglect their Feshbach coupling through the continuum still, and compare them with the CCR results. We see a dramatic increase in the cross section through the higher-energy resonance $3s3d(^1D)7f\,^2F^o$. The two $^2F^o$ resonances are in fact highly mixed but we continue to label them as in the single configuration approximation. The reason for this increase in the resonant-excitation cross section becomes apparent when we examine the autoionization rates in detail. In Table I we compare the autoionization rates contributing to each reso-
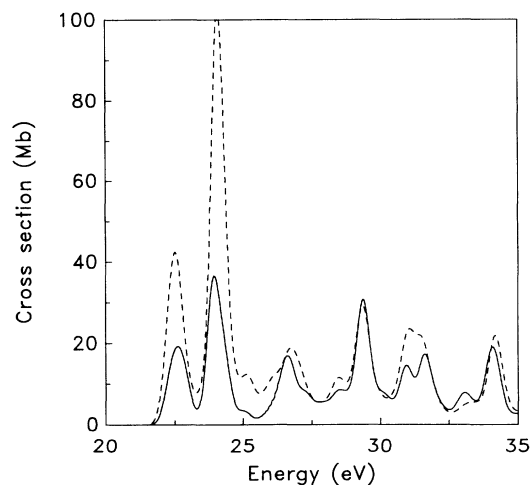

FIG. 6. Electron-impact excitation cross sections for the $3s^2\,^1S\rightarrow 3s3p\,^3P$ transition in Ti^{10+}, convoluted with a 0.5-eV FWHM Gaussian function. Eight-state calculations including the $3s^2\,^1S$, $3s3p\,^{1,3}P$, $3s3d\,^{1,3}D$, and $3p^2\,^1S$, ^3P, and ^1D terms; ——, IPIRDW results; ----, CCR results; both this work.
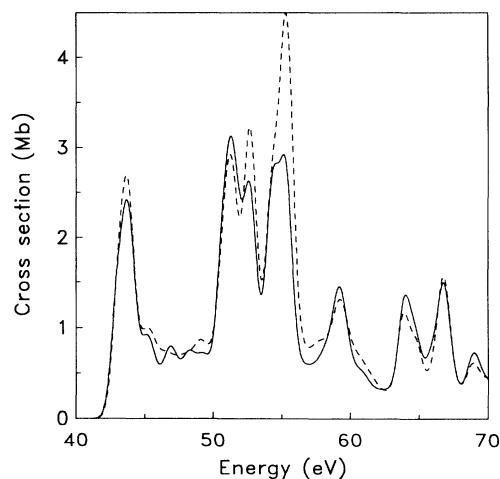

FIG. 8. Electron-impact excitation cross sections for the $3s^2\,^1S\rightarrow 3s3p\,^3P$ transition in Se^{22+}, convoluted with a 1.0-eV FWHM Gaussian function. Eight-state calculations including the $3s^2\,^1S$, $3s3p\,^{1,3}P$, $3s3d\,^{1,3}D$, and $3p^2\,^1S$, ^3P, and ^1D terms; ——, IPIRDW results; ----, CCR results; both this work.
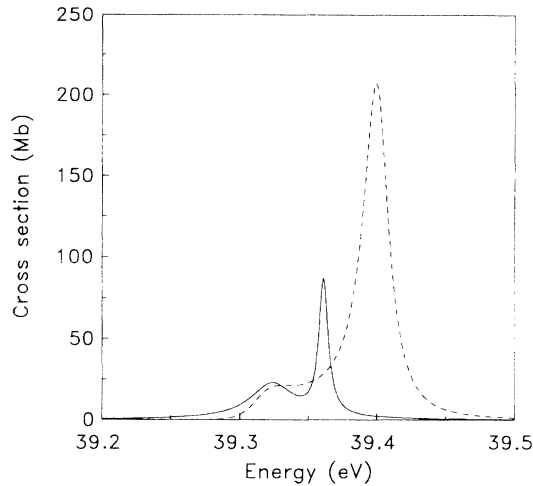
FIG. 9. The $3s3d(^1D)7f\,^2F^o$ and $3s3d(^3D)8p\,^2F^o$ resonances in the $3s^2\,^1S \rightarrow 3s3p\,^3P$ excitation cross section of Fe^{14+}; ——, IPIRDW results; ----, CCR results; both this work.
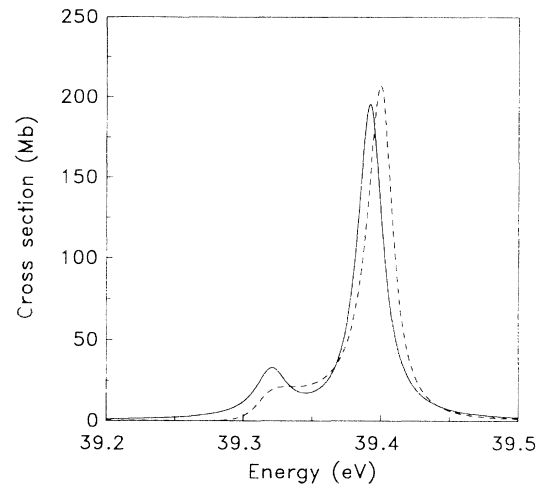
FIG. 10. As Fig. 9, except that direct configuration mixing between the two resonances is now included in the perturbative results.

nance, both with and without direct configuration mixing, where we have summed over the continuum electron angular momenta. We also compare the resulting resonant-excitation cross section energy-averaged over an arbitrary bin-width. The resonant-excitation cross section is most sensitive to changes in the weaker of the entrance-channel autoionization rate and exit-channel autoionization rate. We see that the weaker autoionization rate (to the $3s^2\,^1S$ continuum) for the $3s3d(^3D)8p\,^2F^o$ resonance hardly changes between the mixed and unmixed results. However, the weaker autoionization rate (to the $3s3p\,^3P$ continuum) for the $3s3d(^1D)7f\,^2F^o$ resonance is increased by a factor of 20 due to mixing with the much stronger rate (to the $3s3p\,^3P$ continuum) for the $3s3d(^3D)8p\,^2F^o$ resonance and this results in a factor of 6 increase in the resonant-excitation cross section through the $3s3d(^1D)7f\,^2F^o$ resonance. The $3s3d(^3D)8p\,^2F^o$ autoionization rate (to the $3s3p\,^3P$ continuum) is correspondingly reduced by this mixing but this only results in a small (5%) decrease in the resonant-excitation cross section through the $3s3d(^3D)8p\,^2F^o$ resonance. Next, we

compared our perturbative interacting resonance results both with and without coupling through the continuum, both including direct configuration mixing. We found that there was only a small difference between the two sets of results, mainly to the shape of the resonances than to the integrated cross section (the area under the curve). The resonances need to be physically overlapping before (destructive) interference through the continuum strongly affects the integrated cross sections; this point was noted in our earlier study on dielectronic recombination [8].

The structure at 29 eV is due to resonances of the form $3s3d(^3D)7l$ and $3s3p(^1P)14l'$ and it has been the subject of a recent preliminary examination by Griffin et al. [10]. The differences between the IPIRDW and CCR results are due to a number of the $LS\pi$ symmetries, predominantly $^2F^o$, ^2G, $^2H^o$, and ^2I. In their study of the $^2H^o$ symmetry, Griffin et al. [10] found that the behavior of interacting resonances due to direct configuration mixing and coupling through a common continuum was similar to that which we have observed for the $^2F^o$ at 39 eV. Furthermore, they also studied direct configuration mix-

TABLE I. Energy levels, autoionization rates, and energy-averaged resonant-excitation cross sections $\Delta E \langle \sigma_{RE} \rangle$ (in Mb eV) for the $3s3d(^3D)8p\,^2F^o$ and $3s3d(^1D)7f\,^2F^o$ resonances in the $3s^2\,^1S \rightarrow 3s3p\,^3P$ transition of Fe^{14+}. The numbers in brackets denote multiplicative powers of ten.

Direct configuration mixing	Energy (eV)	$A_a(3s^2\,^1S + e^-)$	$A_a(3s3p\,^3P + e^-)$	$\Delta E \langle \sigma_{RE} \rangle$
		$3s3d(^3D)8p\,^2F^o$		
No	39.324	1.55 [12]	5.69 [13]	1.33
Yes	39.321	1.49 [12]	4.15 [13]	1.26
		$3s3d(^1D)7f\,^2F^o$		
No	39.362	1.11 [13]	1.35 [12]	1.06
Yes	39.392	1.18 [13]	2.15 [13]	6.71

ing as a function of resonance separation and found, even at a separation of several times the mean resonance width, that direct configuration mixing caused a significant enhancement of the resonance cross section [10]. Continuing their study of the resonances at 29 eV, we find that direct configuration interaction also accounts for the discrepancies between the IPIRDW and CCR results for the $^2F^o$ and ^2G symmetries. However, two pairs of resonances of the ^2I symmetry, namely $3s3d(^3D)7g$ plus $3s3d(^3D)7i$ and $3s3p(^1P)14h$ plus $3s3p(^1P)14k$, are overlapping, and destructive interference due to continuum coupling between the two pairs reduces the contribution from this symmetry by a factor of 3; there is little interaction within each pair. Our perturbative results for these resonances, both with and without continuum coupling but including direct configuration interaction, are compared with our four-state CCR results in Fig. 11; note that the resonances are completely overlapping and are not distinguishable even when energy resolved by their natural widths. Despite the sensitivity of the continuum coupling to the resonance separation, we see that our perturbative approach and our treatment of energy corrections gives results in very good agreement with those of the nonperturbative R-matrix method.

Finally in Fig. 12 we can now compare our eight-state R-matrix results for the total $3s^2\,^1S \rightarrow 3s3p\,^3P$ cross section in Fe^{14+} with our perturbative results that include direct configuration mixing (but continuum coupling only for the case just described) between the resonances lying at about 29, 39, and 42.5 eV only; the enhancement of the latter peak is due to mixing between $3s3d\,^3D8l$ and $3p^2\,^1D10l'$, for several $SL\pi$ symmetries. We see that we have now removed the major discrepancies between the IPIRDW and R-matrix results that we noted previously [9]. Before tackling the remaining ions, or indeed the
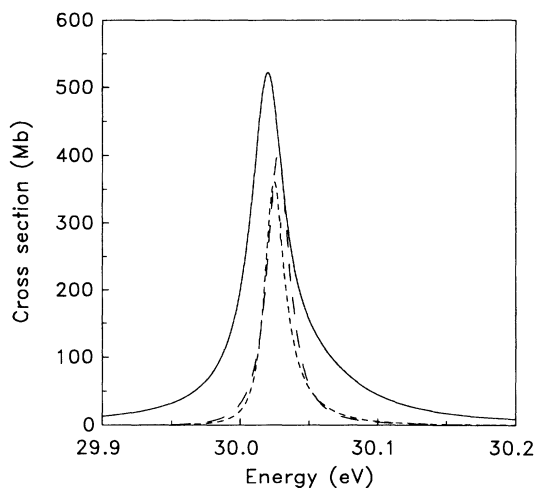

FIG. 12. Eight-state electron-impact excitation cross sections for the $3s^2\,^1S \rightarrow 3s3p\,^3P$ transition in Fe^{14+}, convoluted with a 0.5-eV FWHM Gaussian function. ----, CCR results; ——, perturbation theory results partially allowing for direct configuration mixing and continuum coupling (see text for details); both this work.

FIG. 11. The $3s3d(^3D)7g$ plus $3s3d(^3D)7i$ and $3s3p(^1P)14h$ plus $3s3p(^1P)14k$ resonances of the ^2I symmetry in the $3s^2\,^1S \rightarrow 3s3p\,^3P$ excitation cross section of Fe^{14+}. ——, perturbative results excluding coupling through the continuum; ----, perturbative results including coupling through the continuum (both include direct configuration mixing). − − −, CCR results. All this work.
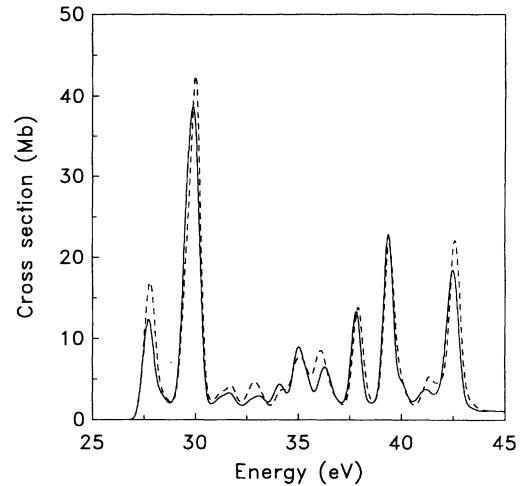
small discrepancies that remain for Fe^{14+}, we plan to develop a more automatic and ab initio computational approach to direct configuration mixing and, where necessary, continuum coupling. This would involve a preliminary pass through the list of resonant states to identify those of a given $SL\pi$, or $J\pi$ in intermediate coupling [15], that lie sufficiently close in energy to warrant subsequent direct configuration interaction and possibly continuum coupling. Thus far, our studies have only necessitated the interaction of pairs of resonances from different complexes (but the computer code is set up for an arbitrary number). Even with more complex ions it is likely that only a few states will need to be interacted, i.e., we do not need to diagonalize the entire Rydberg series and so the problem should remain tractable.

The interacting resonance effects studied in this paper are expected to be of less importance for dielectronic recombination than for electron-impact excitation, and indeed the many comparisons between theory and experiment do not show widespread differences. First, dielectronic recombination cross sections are inherently insensitive to the autoionization rates and they are most frequently proportional to the radiative rates which are dominated by core transitions and for which full configuration mixing is always included. Secondly, direct configuration mixing can affect resonant excitation either via the entrance-channel or exit-channel autoionization rates (as in Table I) while for dielectronic recombination it must affect the entrance channel to be important; alternative autoionization exit channels generally suppress dielectronic recombination cross sections to such an extent that there is no significant contribution when they are present.

Although we have demonstrated the importance of allowing for interacting resonances and identified direct

configuration mixing as the predominant mechanism rather than coupling through a common continuum, as yet, we do not know the accuracy of our description of them. For example, we have noted the sensitivity of the interacting resonance effects to the resonance separation. Although the perturbative and nonperturbative approaches of adjusting the target energies before diagonalization of the $(N+1)$-electron Hamiltonian give resonance positions in good agreement with each other, we do not know their absolute accuracy and hence the uncertainty in the resulting cross section to this approach. Also, the results presented here are for the nonrelativistic LS-coupling problem. Although the term energies were adjusted to the weighted mean of the observed levels, future studies require similar calculations to be carried out in intermediate coupling using the Breit-Pauli Hamiltonian. This may well change the quantitative nature of the results but the qualitative effects of interacting resonances will remain. In light of this, it would be highly desirable to have some experimental results so as to be able to benchmark theory. We note that the electron energy-loss spectroscopy experiment at Oak Ridge National Laboratory has recently made measurements for the electron-impact excitation of Ar^{7+} at low energies [21]. Similar measurements for Ar^{6+} would enable us to benchmark the nonrelativistic theory.

IV. CONCLUSION

We have presented IPIRDW and CCR results for the electron-impact excitation of the $3s^2\,^1S \rightarrow 3s3p\,^3P$ transition in the Mg-like ions Ar^{6+}, Ti^{10+}, Fe^{14+}, and Se^{22+}. We have demonstrated the widespread effect of interacting resonances and identified direct configuration mixing rather than coupling through the continuum as the predominant effect. We have demonstrated that the perturbative interacting resonance approach within the IPDW approximation gives very good agreement with the nonperturbative approach using the R-matrix method. We have noted the sensitivity of the interacting resonance effects to the resonance separations and hence (relative) positions. Except for the simplest of systems, we expect direct configuration interacting resonance effects to be of importance for all transitions that have large resonance contributions (i.e., nondipole transitions). Their effect on total rate coefficients will be of most importance at low temperatures where a few resonances can dominate the rate coefficient. Less frequently, it will be necessary to allow for interactions through a common continuum, e.g., to examine discrepancies between theory and high-energy resolution experiments, since the resonances need to be physically overlapping before such interactions are significant. Electron-impact excitation cross sections are more sensitive to interacting resonance effects than dielectronic recombination cross sections. A more automatic procedure for including direct configuration mixing and coupling through the continuum is needed in order to treat those cases for which radiation damping is important, since the effect of the radiative operators is not included in the present formulation of the close-coupling approximation.

APPENDIX

As noted in Sec. II, the R-matrix method provides a solution of the close-coupling equations inside the inner region $r < r_a$. In the outer region $(r \geq r_a)$, defined to be the region where the short-range atomic potentials can be neglected, the close-coupling equations reduce to differential equations coupled by long-range multipole potentials. The approach of Seaton and co-workers [17,22], as implemented in the computer program STGF of the Opacity Project R-matrix codes [17], is to retain only the dipole and quadrupole potentials and to treat them as perturbations. The differential equations to be solved in the outer region are then just those for the Coulomb functions $y(\varepsilon,l;r)$, viz.,

$$\left[\frac{d^2}{dr^2} - \frac{l(l+1)}{r^2} + \frac{2}{r} + \varepsilon\right]y = 0 , \qquad (A1)$$

where, following Seaton and co-workers [17,22], the z dependence need not be considered explicitly. Solutions of Eq. (A1) are required for numerical integration of the long-range multipole integrals over the range $[r_a,r_2]$, where r_2 is the point at which the asymptotic methods of Sil, Crees, and Seaton [23] can be used to complete the integration over the range (r_2,∞). Closed-channel solutions $\theta(\varepsilon,l;r)$, i.e., $\varepsilon = -v^{-2}$, where v is the effective quantum number, and $\dot\theta$ (where the overdot denotes the differential with respect to ε) are integrated numerically from their outer-turning point r_o, where their exponential asymptotic form is known, inwards to the R-matrix boundary at r_a. For $\varepsilon l(l+1) > -1$, the outer-turning point is given by

$$r_o = -\{[1+\varepsilon l(l+1)]^{1/2}+1\}\varepsilon^{-1} , \qquad (A2)$$

and so $r_o \approx 2v^2$ for $\varepsilon l(l+1) \ll 1$ and thus $r_o \rightarrow \infty$ as $\varepsilon \rightarrow 0^-$. At some energy below every threshold, using a finite radial mesh, r_o exceeds the mesh available $(r_o > r_{max})$ and it is not possible to evaluate $\theta,\dot\theta,\theta',\dot\theta'$ at r_o to start off the inward numerical integration and hence obtain solutions for θ and $\dot\theta$ over the range $[r_a,r_2]$ (since $r_2 \geq r_o$); here the prime denotes the differential with respect to r. When the solution is unobtainable for one closed channel, STGF switches off the perturbative solution completely until that channel becomes open.

For the case of r_o (and hence r_2) $> r_{max}$, we evaluate θ and θ' at r_a from

$$\theta = -\cos(\pi v)s + \sin(\pi v)c \qquad (A3)$$

and

$$\theta' = -\cos(\pi v)s' + \sin(\pi v)c' , \qquad (A4)$$

where s and c are the Coulomb functions $s(\varepsilon,l;r)$ and $c(\varepsilon,l;r)$; we use the definitions and notation of Seaton and co-workers [17,22] whenever possible. Also, from Eq. (A3) we have that

$$\dot{\theta} = \frac{v^3}{2}[\pi\sin(\pi v)s - \cos(\pi v)\dot{s} + \pi\cos(\pi v)c$$

$$+\sin(\pi v)\dot{c}]\ ,\tag{A5}$$

but s and c vary slowly with energy (at $r=r_a$) and so we set $\dot{c}=0=\dot{s}$ and thus obtain

$$\dot{\theta} = \frac{v^3}{2}[\pi\sin(\pi v)s + \pi\cos(\pi v)c] = \frac{\pi v^3}{2}\xi\ ,\tag{A6}$$

where θ and ξ are two linearly independent solutions of Eq. (A1); see Ref. [22]. Finally, ultilization of the Wronskian at $r=r_a$,

$$\theta\dot{\theta}' - \theta'\dot{\theta} = 1\ ,\tag{A7}$$

enables us to complete the evaluation of $\theta,\dot{\theta},\theta',\dot{\theta}'$ at $r=r_a$. This is sufficient to enable us to integrate θ and $\dot{\theta}$ outwards from r_a to $r_{\max}$ and since $r_o>r_{\max}$ we do not encounter any numerical problems due to the exponentially increasing closed-channel solution. We note that the power-series expansion for the Coulomb functions (and hence θ) cannot be applied at large r due to cancellation error, further necessitating the above approach. Finally, we then neglect the contribution to the long-range multipole integrals from r over the range $(r_{\max},\infty)$, only for those integrals involving closed channels θ with $r_o>r_{\max}$. In all of the cases examined so far, with a suit-

ably large $r_{\max}$, we observe no discontinuity in our cross sections as we pass from small negative energies through to small positive energies.

We note that a similar problem can occur in the evaluation of the open-channel long-range integrals for the case of small positive energies, coupled with large angular momentum. Here, the inner turning point r_i can move out beyond r_a. The Coulomb function s is then unstable to inwards integration and so must be integrated outwards from r_a. The worst case is encountered for $\varepsilon=0$; then the inner turning point is given by

$$r_i = \tfrac{1}{2}l(l+1)\ .\tag{A8}$$

But from Eq. (A8), we see that we can again encounter the situation of $r_2>r_{\max}$ (since $r_2>r_i$), this time for large l; when this happens STGF again switches off the perturbative solution in the outer region for all channels. The situation is not as bad, in principle, as for the closed-channel case discussed above since we are always dealing with finite l and hence require a finite $r_{\max}$. But in practice, $r_{\max}$ becomes excessively large for the high l (e.g., $l\sim 60$) encountered in the solution of the close-coupling equations using the nonexchange R-matrix code [24]. Our solution is to proceed as in the existing case of $r_{\max}>r_2$ so as to obtain a solution over the range $[r_a,r_{\max}]$ and then again to neglect the contribution to the long-range multipole integrals from r over the range $(r_{\max},\infty)$, only for the integrals involving the affected open channel.

[1] P. G. Burke and W. D. Robb, Adv. At. Mol. Phys. **11**, 143 (1975).

[2] M. Gailitis, Zh. Eksp. Teor. Fiz. **44**, 1974 (1963) [Sov. Phys. JETP **17**, 1328 (1963)].

[3] K. Sakimoto, M. Terao, and K. A. Berrington, Phys. Rev. A **42**, 291 (1990).

[4] R. J. W. Henry and L. Lipsky, Phys. Rev. **153**, 51 (1967).

[5] R. D. Cowan, J. Phys. B **13**, 1471 (1980).

[6] M. A. Hayes and M. J. Seaton, J. Phys. B **10**, L573 (1977).

[7] N. R. Badnell, M. S. Pindzola, and D. C. Griffin, Phys. Rev. A **43**, 2250 (1991).

[8] M. S. Pindzola, N. R. Badnell, and D. C. Griffin, Phys. Rev. A **46**, 5725 (1992).

[9] N. R. Badnell, D. C. Griffin, T. W. Gorczyca, and M. S. Pindzola, Phys. Rev. A **48**, R2519 (1993).

[10] D. C. Griffin, M. S. Pindzola, F. Robicheaux, T. W. Gorczyca, and N. R. Badnell, Phys. Rev. Lett. **72**, 3491 (1994).

[11] D. C. Griffin, M. S. Pindzola, and N. R. Badnell, Phys. Rev. A **47**, 2871 (1993).

[12] J. M. Blatt and L. C. Beidenharn, Rev. Mod. Phys. **24**, 258 (1952).

[13] This is the normalization used by the AUTOSTRUCTURE code; a variety of alternatives can be found in the literature, e.g., either one or $(\pi k)^{-1/2}$ times a sine function.

[14] W. Eissner, M. Jones, and H. Nussbaumer, Comput. Phys. Commun. **8**, 270 (1974).

[15] N. R. Badnell, J. Phys. B **19**, 3827 (1986).

[16] H. Feshbach, Ann. Phys. (N.Y.) **5**, 237 (1958); **19**, 287 (1962); **43**, 421 (1967).

[17] K. A. Berrington, P. G. Burke, K. Butler, M. J. Seaton, P. J. Storey, K. T. Taylor, and Yu Yan, J. Phys. B **20**, 6379 (1987).

[18] M. S. Pindzola and N. R. Badnell, Phys. Rev. A **39**, 1685 (1987).

[19] C. Froese Fischer, Comput. Phys. Commun. **64**, 369 (1991).

[20] R. L. Kelly, J. Phys. Chem. Ref. Data **16**, Suppl. 1 (1987).

[21] X. Q. Guo, E. W. Bell, J. S. Thompson, G. H. Dunn, M. E. Bannister, R. A. Phaneuf, and A. C. H. Smith, Phys. Rev. A **47**, R9 (1993).

[22] M. J. Seaton, Rep. Prog. Phys. **46**, 167 (1983).

[23] N. C. Sil, M. A. Crees, and M. J. Seaton, J. Phys. B **17**, 1 (1984).

[24] V. M. Burke, P. G. Burke, and N. S. Scott, Comput. Phys. Commun. **69**, 76 (1992).